Poster Abstracts from the Molecular Neuroimaging Symposium

SNM and the SNM Molecular Imaging Center of Excellence (MICoE) are sponsoring a symposium designed to help disseminate the latest molecular neuroimaging research and the most promising related clinical applications. The Molecular Neuroimaging Symposium will be held this month at the National Institutes of Health (NIH) and will include lectures from invited experts in the field, panel discussions, and a poster session. This multidisciplinary meeting is attracting individuals from both the basic science and the clinical communities. In this special section of *JNM*, we are publishing the 26 original abstracts selected for poster presentation at this symposium.

The application of molecular imaging will provide unique insights, making possible a more personalized approach to the evaluation and management of diseases of the central nervous system (CNS). See www.snm.org/brain2010 for information on the speakers and agenda. This conference is designed to build on a successful symposium on cardiovascular molecular imaging held at NIH in May, 2009 (see *J Nucl Med.* 2010;51(suppl 1)).

Speakers have been chosen from multiple scientific disciplines, including chemistry, engineering, physics, molecular biology, neurosciences, and imaging sciences. This symposium will focus on advances in targeted multimodality imaging of the central nervous system and will cover imaging of the blood–brain barrier (BBB), tumors, neuroreceptors, stem cells, adoptive immunotherapies, and other biological processes relevant to the CNS. This gathering of leading researchers will foster collaborations between participants and stimulate further interest in this rapidly evolving field.

The abstracts presented here represent some of the most interesting ideas in molecular imaging research as applied to the CNS. We have put particular emphasis on encouraging participation by junior scientists. The first section contains those abstracts selected to receive Young Investigator Travel Awards* sponsored by the MICoE, the Society of Radiopharmaceutical Sciences, and the Society for Molecular Imaging. Abstracts are also presented related to new molecular probes and imaging technologies, as well as preclinical and clinical applications of molecular imaging.

Michelle Bradbury, MD, PhD
Memorial Sloan-Kettering Cancer Center
PI and Organizing Committee Member

Dima Hammoud, MD
National Institute of Health/Clinical Center
Organizing Committee Member

Abstract Reviewers

*Young Investigator abstracts are listed alphabetically by first author in section 1.

SECTION 1

Young Investigator Travel Award Winners

1***

Increased L-[1-^{11}C]leucine Uptake in the Angioma Associated with Cortical Hypometabolism in Children with Sturge-Weber Syndrome: a PET Study. B. Alkonyi[1], C. Juhasz[1], H.T. Chugani[2], O. Muzik[2], D. Chugani[2], S. Sundaram[2], W. Kupsky[3], C. Batista[1]; 1. Children's Hospital of Michigan, PET Center, Wayne State University, Detroit, Michigan; 2. Wayne State University, Departments of Pediatrics, Neurology, Radiology, Detroit, MI; 3. Wayne State University, Department of Pathology, Detroit, Michigan

Objectives: Endothelial proliferation and vascular remodeling in the leptomeningeal angioma may contribute to clinical progression in Sturge-Weber syndrome (SWS). In this study, we used positron emission tomography (PET) to explore if increased amino acid uptake, often associated with increased cell proliferation, is present in the angioma region in children with SWS. **Methods:** PET scanning with L-[1-^{11}C]leucine (LEU) was performed in 7 children (age: 5 months-13 years) with unilateral SWS. Asymmetries of standard uptake values (SUVs) of LEU uptake in the posterior (angioma) region as well as in frontal cortex were measured and also correlated with glucose metabolic abnormalities measured by glucose PET. Further kinetic analysis of LEU uptake was performed in 4 cases to evaluate mechanisms of LEU uptake. **Results:** Increased LEU SUV values were found in the posterior region in 6 patients (mean increase: 15.1 %) and less pronounced increases were seen in frontal cortex in 4 (mean: 11. 5 %). Increased LEU uptake was mainly driven by increased tracer transport. Increased protein synthesis rates were measured in two young patients aged 2.4 and 2.9 years. Higher LEU SUV asymmetries were associated with more severe hypometabolism in the posterior region (r=-0.82, p=0.046). Signs of endothelial cell proliferation and angiogenesis were seen in resected angioma of an infant who underwent epilepsy surgery. **Conclusions:** Increased LEU transport and protein synthesis rates in the angioma regions may be related, at least partially, to proliferative activity due to active vascular remodeling in children with SWS. Increased protein synthesis in the angioma of young children with SWS may be a marker of disease activity contributing to chronic brain damage.

2**

Design and Synthesis of Boron Containing Retinoids as New Therapeutic and Diagnostic agent for Brain Cancer Glioblastoma Multiforme (GBM). B.C. Das, L. Agoni, C. Guha; Albert Einstein College of Medicine, Bronx, New York

Objectives: The objective of this study to develop new therapeutic and diagnostic agents for brain cancer. Glioblastoma multiforme (GBM) is a very aggressive brain tumor for which cure is exceptionally rare. Despite advances in neurosurgical techniques and in radiation and drug therapies, glioblastoma multiforme has a dismal prognosis. Surgery and radiation are limited by the interdigitation of tumor cells into healthy brain, resulting in imprecise treatment boundaries. Current treatment using adjuvant chemotherapy with radiation after surgery has resulted in small improvements in time to progression for most patients. Retinoic acid receptor alpha (RARα) is well described as over expressed in GBM. The RAR pathway elicits differentiation and apoptosis in cancer cells. Unfortunately treatments based on all-trans-retinoic acid (atRA) have not been proven effective and also burdened with high toxicity. We designed and synthesized retinoid analogues based on structure activity relation studies (SAR) of retinoic acid receptor alpha (RARα) and tested their biological activity in vitro U87 glioblastoma cells. **Methods:** Based on SAR and modeling studies we designed and synthesized new retinoic acid analogues by introducing a constrained phenyl ring system in the place of conjugated alkene backbone (spacers in ATRA) to inhibit the metabolism of ATRA into its isomers, 9-CRA and 13-CRA and then tested their biological activity against U87 cells. In order to investigate the activity of the compounds, Alamar Blue (Biotium Inc. Hayward, CA) viability assay was used and the concentration inhibiting the growth of 50% of the cells (IC_{50}) determined. Western blot was used to verify the nuclear level of RARα and detection of histone H1 was used as loading control. U87 cells were incubated for 24, 48 and 72 hours either with BC-128 10μM, atRA 10μM, atRA 60μM, atRA 10μM+BC-128 10μM or equal volume of DMSO for control. Afterward cells were harvested and nuclear fraction obtained for protein determination. **Results:** Among the compounds synthesized, we selected BC-128 as the most active. BC-128 proved to be several times more active than atRA, with IC_{50} of 10μM and 60μM respectively. Western blots showed that prolonged incubation of atRA led to down regulation of RARα, therefore limiting the pro-apoptotic and differentiating effect of the retinoic acid pathway. BC-128 not only did not cause RARα down regulation but prevented it when incubated with atRA. **Conclusions:** From our initial screening we selected our lead molecule, BC-128, which exhibited cytotoxic effect in U87 cell lines in a micro-molar range. Further studies are ongoing to clarify all the interactions between BC-128 and the retinoic acid pathway, and to prove its efficacy on broader in vitro and in vivo settings. Moreover, BC-128 will be used as model compound to iterate the process to synthesize additional compounds with similar characteristics and higher anti-tumor activity. In future these compounds could be radio labeled ^{11}C or ^{18}F to use as novel diagnostic agent. As these compounds contain boron atom, they will potentially in future could be used as BNCT (Boron Neutron Capture Therapy Agent).

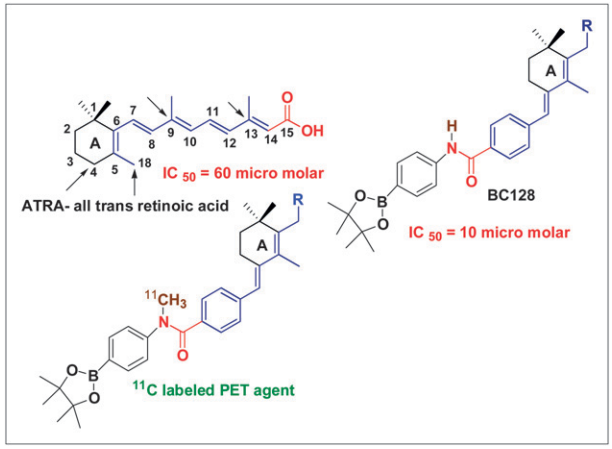

FIGURE 1. Structure of atRA, BC128 and future radio labeled compound

3*

Magnetic Resonance Imaging of Intracranial Tumors: Intra-Patient Comparison of Gadoteridol and Ferumoxytol. E. Dósa, M. Haluska, C. Lacy, S. Gahramanov, J. Njus, W. Rooney, E. Neuwelt; Oregon Health and Science University, Portland, Oregon

Objectives: To prospectively compare gadoteridol (Gd) and ferumoxytol (Fe) for contrast-enhanced and perfusion-weighted (PW) MRI of intracranial tumors. **Methods:** The final analysis included 27 patients (19 men) with a mean age of 47.9 years, who underwent 3T MRI (2008 to 2009). The imaging protocol consisted of 3 consecutive days. On the first day, axial T1W SE and T2W TSE pre- and postcontrast images, and PW MRI were acquired using Gd. On the following day, the same MRI sequences were obtained with Fe; and on the third day the anatomical images were repeated in identical spatial orientation to detect the delayed Fe enhancement. Gd was injected at a dose of 0.1 mmol/kg; Fe was given in a constant volume of 17 mL (510 mg) diluted with 17 mL of saline, from which an initial 5 mL bolus was used for PW MRI. The T1W images were evaluated qualitatively and quantitatively [enhancement volume, lesion-to-brain contrast-to-noise ratio (CNR), signal intensity (SI) change]; PW data were used to estimate relative cerebral blood volume (rCBV) ratio. **Results:** All lesions showed 24-hr Fe-induced T1W SI changes, but only 17 of them had T2W hypointensities in the approximate region where T1W Gd enhancement was seen. Six patients had T1W Fe enhancement even in areas of no Gd enhancement. Side-by-side analysis of T1W postcontrast images

*Travel award sponsored by the SNM Molecular Imaging Center of Excellence.
**Travel award sponsored by the Society of Radiopharmaceutical Sciences.
***Travel award sponsored by the Society for Molecular Imaging.

has revealed that the morphology of Gd enhancement was more homogeneous compared with the hazy, punctuate pattern of Fe enhancement. The qualitative analysis (lesion delineation, lesion internal morphology, lesion enhancement) has showed significant preferences (P= .0118; P= .0010; P < .0001, respectively) for Gd compared with Fe. There was no significant difference (P= .4506) in enhancement volumes of the lesions measured on T1W Gd- and 24-hr Fe-enhanced images. A significant difference (P< .0001) was demonstrated among the CNRs obtained on T1W precontrast, Gd- and 24-hr Fe-enhanced images. Significantly greater (P< .0001) SI changes were seen with Gd than with Fe. The Fe-rCBV values were significantly higher (P= .0008) compared with the Gd-rCBV values. **Conclusions:** The 24-hr Fe enhancement was different from the Gd enhancement in morphology and intensity; presumably because of these nanoparticles are taken-up by inflammatory cells. As Fe is a blood pool agent, we assume that the rCBV measurements are more accurate with Fe than with Gd.

4***

Evaluation of neuroinflammation in children with Niemann Pick disease type-C using [C-11] PK-11195 PET. A. Kumar[1], H. Chugani[2], P. Chakraborty[2], O. Muzik[2]; 1. Children's Hospital of Michigan, PET Center, Wayne State University School of Medicine, Detroit, Michigan; 2. Wayne State University School of Medicine, Detroit, Michigan

Objectives: Neuroinflammation, mediated by activated microglia, has been reported in the globus pallidus, thalamus and cerebellum of Niemann-Pick disease type-C (NPC) -/- mice brain, occurring early in the disease course, prior to any signs of neuronal pathology or overt clinical symptoms (Baudry M, et al., Exp Neurol 2003). However, it is difficult to evaluate neuroinflammation in humans, as *in vivo* confirmation of microglial activation traditionally requires pathological examination of tissue. Since activated microglia can be imaged with the PET tracer [C-11] PK-11195 (PK), which binds to peripheral benzodiazepine receptors (PBR) expressed by these cells, PK PET can be used for *in vivo* evaluation of activated microglial mediated neuroinflammation. **Methods:** Eight NPC patients (age: 8.2 ± 3. 9 (4-16) years; 5 females) and 7 healthy adults (age: 27.4 ± 7.5 years, 3 females) underwent dynamic PET imaging of brain after injection of 17 MBq/kg of PK and binding potential (BP: a semiquantitative measure of PK binding to PBRs) was calculated in basal ganglia, thalamus and cerebellum. **Results:** BP was found to be significantly increased in the basal ganglia (0.22 ± 0.1 Vs 0.14 ± 0.04) and thalamus (0.42 ± 0.11 Vs 0.3 ± 0.08) in children with NPC compared to normal controls (p=0.02 and 0.006, respectively). Although BP was also higher in the cerebellum of NPC children (0.18 ± 0.2) compared to that of normal controls (0.09 ± 0.06), the difference was statistically not significant (p=0.15). PK abnormalities also appeared to correlate with clinical manifestations. **Conclusions:** Our findings support increased activated microglial cells in the basal ganglia and thalamus of children with Niemann Pick disease type C, suggesting underlying neuroinflammation, which can be shown *in-vivo* with PK PET. Therefore, it appears that PK PET may be used as a biomarker in this condition; however, further prospective studies and neuropathologic correlations are required to confirm its value in monitoring progression and response to interventions.

5**

Differential diagnosis of Parkinson's disease and drug-induced parkinsonism using F-18-FP-CIT PET/CT. E. Park[1], P. Kun Woo[1], Y.M. Hwang[2], J.G. Choe[1]; 1. Korea University Anam Hospital, Korea University College of Medicine, Department of Nuclear Medicine, Seoul, Korea; 2. Dongguk University, Department of English Language, Interpretation & Translation, Seoul, Korea

Objectives: Evaluation of striatal presynaptic dopaminergic function with SPECT imaging using I-123-β-CIT or I-123-FP-CIT has been proved to be useful in the differential diagnosis of parkinsonism and in the severity assessment of Parkinson's disease. Recently a PET tracer for dopamine transporter (DAT) imaging, F-18-N-(3-fluoropropyl)-2β-carbomethoxy-3β-(4-iodophenyl) nortropane (F-18-FP-CIT), has been approved by Korean FDA, which has superior tracer kinetics and spatial resolution than SPECT tracers. We investigated the usefulness of F-18-FP-CIT PET/CT imaging in the differential diagnosis of patients with parkinsonism. **Methods:** Twenty-seven clinically diagnosed Parkinson's disease (PD) patients (mean age 67.0 ± 9.9 y, M: F=8: 19), 6 patients with drug-induced parkinsonism (DIP) (74. 5±9.2 y, M: F=2: 4), and 8 age-matched normal controls (65.1±4. 7 y, M: F=2: 6) were studied with F-18-FP-CIT PET/CT. F-18-FP-CIT PET/CT images were obtained 120 minutes after injection of 185 MBq F-18-FP-CIT. Semi-quantitative analysis was performed using manual ROI method. A DAT parameter V3", a measure directly related to the density of DAT, was calculated in striatal regions as (striatal ROI-cerebellar ROI mean radioactivity)/cerebellar ROI mean radioactivity on F-18-FP-CIT PET/CT images. **Results:** In patients with PD, V_3" in the caudate nucleus (2. 69±0.69) and putamen (2. 10±0.84) was significantly lower than those of DIP patients (3. 69±0.63 and 3. 99±0.66, respectively) and normal controls (3. 88±0.54 and 4. 16±0.61, respectively) (p<0.05). There was no significant striatal V_3" difference between DIP patients and normal controls. The ratio of putamen-to-caudate nucleus V_3" of PD patients (0.77±0.18) was significantly lower than those of DIP (1. 09±0.08) and normal controls (1. 07±0.09) (p<0.05), indicating that putamen is more affected than caudate nucleus in PD. See Figure. **Conclusions:** Evaluation of striatal DAT density with F-18-FP-CIT PET/CT imaging was useful in the differential diagnosis of PD and DIP. Supported by Korea University Grants (K0932081, K0931131).

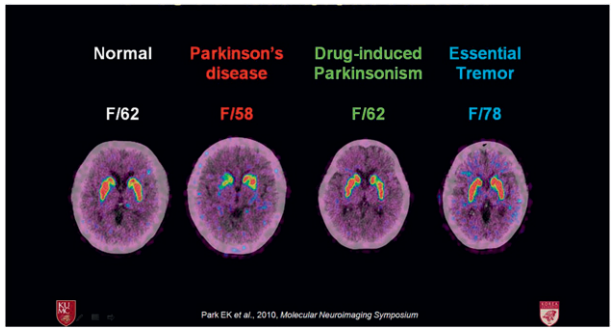

FIGURE 1. F-18 FP CIT Brain PET/CT comparing normal brain with Parkinson's disease, drug-induced parkinsonism and essential tremor.

6*

Disruption of Functional Brain Connections in Alzheimer's Disease. F.C. Sheldon[1], J. Petrella[2], P.M. Doraiswamy[2]; 1. Duke University Medical Center, Dept of Radiology, Durham, North Carolina; 2. Duke University Health System, Durham, North Carolina

Objectives: To identify brain regions in which memory task-related functional brain connections are disrupted with the progression of Alzheimer's Disease. **Methods:** 13 patients with mild AD, 11 patients with prodromal AD (pAD), 23 patients with stable mild cognitive impairment (sMCI), and 28 elderly controls (ONS) underwent functional MR imaging during a face-name associative encoding-retrieval task. The designations of pAD and sMCI were established in MCI patients after a 2. 5 year clinical follow up. Images were normalized to a standardized brain template (Montreal Neurologic Institute) using statistical parametric mapping software (SPM 5). Datasets were also masked to include only gray matter voxels, using the WFU PickAtlas gray matter region of interest dilated by a factor of 2. For assessment of functional brain connections in the fMRI cohort, voxelwise weighted degree maps were created for each subject by constructing a correlation matrix including all graymatter voxels. A weighted measure of connectivity for each voxel was then obtained by summing the correlation of the time-course of a given voxel in gray matter with that of every other voxel in gray matter. Each connection map was normalized to the global mean for that individual by converting weighted correlation coefficients to z-scores. To assess disruption in functional connectivity with AD progression, a 'disease rank' of 1-4 was assigned for

*Travel award sponsored by the SNM Molecular Imaging Center of Excellence.
**Travel award sponsored by the Society of Radiopharmaceutical Sciences.
***Travel award sponsored by the Society for Molecular Imaging.

patients in the, AD, pAD, sMCI, and ONS categories, respectively. This rank was then used as a covariate in a voxelwise correlation with the normalized weighted connectivity to identify areas which showed functional disruption along with the progression of AD. Voxelwise correlations were carried out in SPM8 using a p-value < 0.05, corrected for multiple comparisons at the cluster level, with a cluster extent threshold of 10 voxels. **Results:** A statistically significant cluster in the right inferior frontal gyrus showed evidence of functional disruption correlating with disease classification. Mean z-scored values of connectivity were found to be 0.75 (ONS), 0.60 (sMCI), 0.27 (pAD), and 0.04 (AD). C**onclusions:** These results demonstrate an area of disruption in functional brain connections during an associative memory task in the right frontal lobe which is related to the progression of AD. Better understanding of such functional changes in the progression of AD may help bridge the gap between our understanding of the molecular underpinnings of AD and its phenotypic manifestations.

7**

Development of dPET, a non-invasive imaging technique to measure the distribution of drugs after direct delivery to the brain,
R.W. Sirianni, R. Carson, M.Q. Zheng, A.S. Rinderle, W.M. Saltzman, Y. Huang; Yale School of Medicine, New Haven, Connecticut

Objectives: Active agents have been delivered directly to the brain to treat or better understand a variety of diseases; however, most techniques used to measure the spatial distribution that results from local delivery are highly invasive. In this work, we use Positron Emission Tomography (PET) to quantify the distribution of compounds that were directly delivered to the brain or brain phantoms. We also report the use of a new tracer ([18F]fluorobenzylamine-poly(ethylene glycol)$_4$-biotin, NPB4) that can be used for rapid, modular radiolabeling of polymers. **Methods:** A variety of F-18 and 11-C radiotracers were directly delivered *in vitro*, to an agarose brain tissue mimic, or *in vivo*, to the striatum or cerebral ventricles of rats. Experimental parameters included a range of radiotracer volumes (5-30μL), infusion rates (0.5-5μL/min), and total activity (1-230 μCi). Imaging sessions were conducted in the Focus 220 scanner. Emission data were collected for 2-6 hrs, binned to appropriate frame durations (0.5-20 min), and reconstructed with OSEM or FBP algorithms. **Results:** Fitting the data to a model of Fickian diffusion produced accurate estimates of the *in vitro* diffusion coefficients of charged and uncharged radiotracers with molecular weights ranging from 18-60,000Da (fig 1). In addition, dPET was used to quantify the diffusion, convection, elimination and immobilization of radiotracers in the brains of anesthetized rats. Transport in the striatum was dominated by high rates of immobilization and elimination for [18F]FDG and [18F]NPB4, although it was possible to measure diffusion with [18F]Fluoride Ion ([18F]F$^-$)a tracer that experiences low binding to soft tissue. [18F]F$^-$ was also used to observe infusion volume-dependent fluid movement through the cerebral ventricles and into the spinal cord (3 hrs). Preliminary results suggest that these methods can be extended to drug-loaded, avidin-coated poly(lactic-co-glycolic acid) (PLGA) nanoparticles. **Conclusions:** This novel imaging method represents an important advancement in the ability to quantitatively and non-invasively explore the barriers to drug transport in the brain. Since the biotin end group on [18F]NPB readily attaches to avidin or avidin-labeled polymer surfaces, [18F]NPB provides useful properties for the non-invasive tracking of delivery vehicles or vectors, such as polymer nanoparticles. We anticipate that dPET will be useful both to design better drug delivery methods as well as to monitor the efficacy of clinically applied therapies.

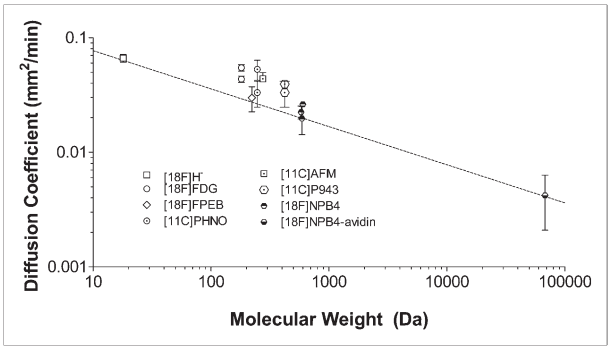

FIGURE 1. Diffusion coefficients of various radiotracers, measured in agarose gel. Each point represents the average of diffusion coefficients obtained at different times during a single imaging experiment. Error bars represent standard deviation. Dashed line indicates theoretical values, based on the Stokes-Einstein relationship.

**Travel award sponsored by the Society of Radiopharmaceutical Sciences.

8**

Novel Imaging Agents for Beta-Amyloid Plaques Based on the 5-(2-Phenylethenyl)-1H-Indole Core. Y. Yang, B.L. Liu; Key Laboratory of Radiopharmaceuticals, Beijing Normal University, Ministry of Education, College of Chemistry, Beijing, P.R.China

Objectives: Alzheimer's disease (AD) is a kind of neurodegenerative disease characterized by dementia, congnitive impairment and memory loss. One of the key pathological features in AD brain is the formation of β-amyloid (Aβ) plaques, which appear as early as 10 to 20 years before any symptoms are obvious. Therefore, non-invasive detection of Aβ plaques using imaging agents will be a powerful tool for early diagnosis AD. Now, design of radiotracers with novel core structures to image Aβ in vivo will be a great challenge. In our present study, we have developed novel agents containing 5-(2-Phenylethenyl)-1H-Indole core as potential ligands for Aβ plaques imaging. **Methods:** Synthesis of 3 and 4 is shown in Figure. Binding affinities of 3 and 4 to Aβ(1-40) and Aβ(1-42) aggregates were measured by inhibition assays using [I-125]TZDM as the radiolabeled standard. Nonspecific binding was measured in the presence of 100 nM TZDM. After the reaction mixture was incubated at 37°c for 2 h, the bound radioactivity to the Aβ aggregates was collected on borosilicate glass fibre filters using a cell harvester and then counted. The half maximal inhibitory concentration (IC50) were analyzed and the inhibition constant (Ki) values were calculated. **Results:** In Aβ(1-42) aggregates binding assays, binding affinity of TZDM was also measured for a comparison with the reported value. K_i of TZDM (4. 2 nM) was similar to the reported value (2. 2 nM). The K_i values of 3 and 4 were 4. 2 nM and 22. 2 nM for aggregates of Aβ(1-40) and 3. 1 nM and 19.7 nM for aggregates of Aβ(1-42). **Conclusions:** The data demonstrares that 3 has higher binding affinity for Aβ plaques. These results have been encouraging, and further studies are planned to develope this core-based [I-125]-labelled derivatives as new potential SPECT tracers for Aβ plaques imaging studies.

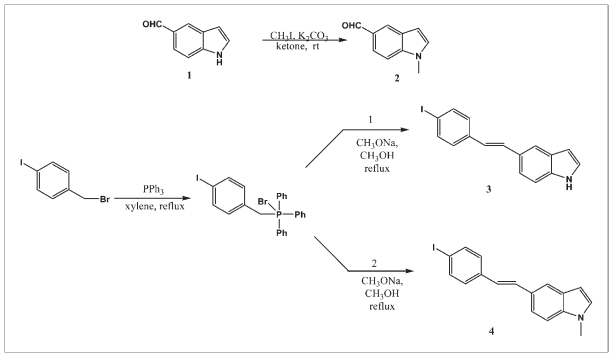

FIGURE 1. Synthesis of 3 and 4.

9**

Novel Indole and Pyrole Derivatives as Potential C-11 Labeled Radiotracer for Imaging β-Amyloid Plaques in AD Brain. L. Yu[1], H. Jia [1], M. Cui[1], M. Scheunemann[2], P. Brust[2], J. Steinbach[2], B.L. Liu[1]; 1. Beijing Normal University, Key Laboratory of Radiopharmaceuticals, Ministry of Education, College of Chemistry, Beijing Normal University, Beijing, P.R. China; 2. Forschungszentrum Dresden-Rossendorf, Research site Leipzig, Interdisciplinary Isotope Research Institute of Radiopharmacy, Leipzig, Germany.

Objectives: Senile Plaques (SPs) and neurofibrillary tangles (NFTs) are two major neuropathological hallmarks in Alzheimer's Disease (AD).The development of new imaging agents for SPs in vivo will play an important role in clinical prediagnosis and the evaluation of clinical treatment. In this work, two series of indole and pyrole derivatives were designed and prepared as new candidate radiotracers aiming at imaging amyloid plaques in AD brain in vivo. **Methods:** Six indole derivatives were synthesized according to the Fisher-indole-reaction from corresponding phenylhydrazine and 1-(4-aminophenyl) ethanone. Four asymmetric 2. 5-diphenylpyrole derivatives were prepared by Suzuki Reaction from Boc-Protected pyrole. Considering the similar chemical structure of IMPY and the new synthesized compounds, [^{125}I]IMPY was selected as standard to measure the following compounds (IN-2, IN-3, IN-5, IN-6, PY-2, PY-3, PY-4)' affinity to β-amyloid plaques by $A\beta_{1\text{-}42}$ aggregates. **Results:** Six indole derivatives and four pyrole derivatives were synthesized successfully. Based on the potential possibility of C-11 labelling, seven Methyl-substituted compounds in aniline-N or pyrole-N were performed with measurement of Ki value. The compounds with double methylation in aniline-N display higher affinity than those with single methylation (IN-3 *vs*.IN-2; IN-6 *vs*.IN-5; PY-3 *vs*.PY-2). Methylation in indole-N or pyrole-N ring reduces the affinity to $A\beta_{1\text{-}42}$ aggregates (IN-5 *vs*.IN-2; IN-6 *vs*.IN-3; PY-4 *vs*.PY-3). The dimethylamino-carried compounds with 2-phenylpyrole ring display the higher affinity to amyloid aggregates than those with indole ring (PY-3 *vs*.IN-3; PY-4 *vs*.In-6). **Conclusions:** The experimental results indicate that In-3, PY-3 and PY-4 have the potential to develop ^{11}C-labelled radiotracers for imaging amyloid plaques in AD brain in vivo.

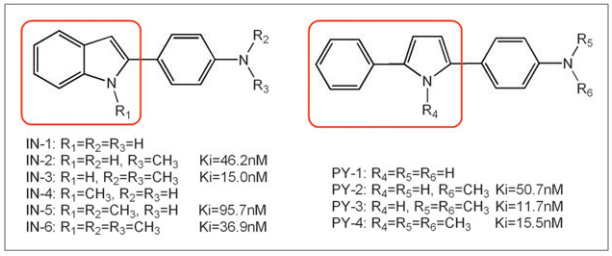

10***

***In vivo* imaging of tumor hypoxia and vasculature of orthotopic mouse brain tumor models.** H. Zhou[1], D. Zhao[2], H. Amyn[2], R. Mason[2]; 1. The University of Texas Southwestern Medical Center, Dallas, Texas; 2. The University of Texas Southwestern Medical Center, Dallas, Texas

Objectives: Malignant brain tumors originating from the brain itself or metastases from breast tumor cells are associated with high morbidity and mortality. Monitoring tumor microcirculation and oxygenation during intracranial development of brain tumors is critical as they play important roles in malignant progression. In addition, hypoxic tumors are more resistant to radiotherapy and other anticancer drugs. We have developed orthotopic brain tumor models of glioma and breast cancer brain metastasis in athymic mice. Here, we are utilizing these models to study interplay of tumor oxygenation and vascular perfusion by applying in vivo imaging approaches.

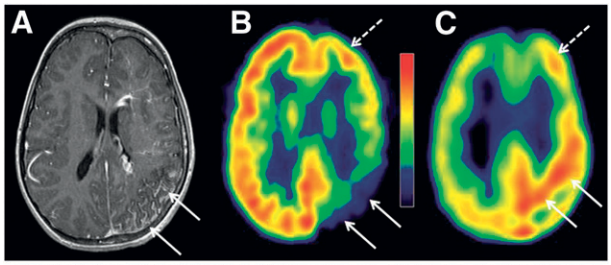

Co-registered T1 postgadolinium MRI (**A**), FDG PET (**B**) and L-[1-^{11}C]leucine (LEU) PET (**C**) images of one of the patients with left hemispheric angioma in the temporo-parieto-occipital region. The angioma region (solid arrow) was hypometabolic but showed increased LEU uptake. The angioma did not extend to frontal cortex; however, this region was also mildly hypometabolic (dashed arrow) and showed moderately increased LEU uptake compared to the contralateral homotopic area.

***Travel award sponsored by the Society for Molecular Imaging.

Methods: Human glioma U87-luc cells and breast cancer MDA-MB-231 cells stably transfected with the hypoxia reporter gene, HRE-ODD-luc were used. 5 x 10^4 U87-luc cells or 1 x 10^5 MDA-MB-231/5HRE-ODD-LUC cells were injected directly into the right caudal nucleus of mouse brain. Bioluminescent imaging (BLI) was used to monitor tumor growth in U87-luc glioma or hypoxia development in MDA-MB-231-HRE-ODD-luc tumors. T_2-weighted and T_1-contrast MR images were acquired to assess tumor volume. Tumor oxygenation was evaluated by Blood Oxygen Level Dependent (BOLD) and Tissue Oxygen Level Dependent (TOLD) MRI. Tumor vascular perfusion and relative regional cerebral blood volume (rCBV) was calculated based on first pass pharmacokinetic modeling (FPPM) acquired using Dynamic Susceptibility Contrast (DSC) MRI. Spatial correlation between these MRI parameters was investigated. **Results:** There was a good agreement between BLI signal intensity and MRI measured tumor volume in U87-luc glioma. Upon oxygen challenge, significant increase in R_2*-weighed signal intensity (SI) was observed in the intracranial tumors in both U87 (mean = 5.2±2. 2 %) and MDA-MB-231 tumors (mean = 1. 6±1. 6%). In line with BOLD MRI, TOLD MRI showed significantly increased SI in both U87 (mean = 5.4 ±1. 7 %) and MDA-MB-231 tumors (mean = 6.0 ± 3. 3%). DSC MRI revealed significantly higher perfusion in tumor than contralateral normal brain in both tumor types. Strong spatial correlation between DSC, BOLD or TOLD was found in three of six U87 tumors. **Conclusions:** Multimodal imaging approaches facilitate studies of both tumor anatomy and pathophysiology of tumor microenvironment.

SECTION 2

11

Drugs for imaging Alzheimer's disease. J. Baranowska-Kortylewicz, Z. Kortylewicz, J. Nearman; University of Nebraska Medical Center, Omaha, Nebraska.

Objectives: to establish noninvasive imaging methods that will aid in validating butyrylcholinesterase (BChE) as a biomarker of Alzheimer's disease (AD) progression and response to therapy. **Methods:** A series of novel BChE inhibitors was designed, synthesized and selected for their reactivity towards BChE. New drugs were fully characterized. Radiolabeling methods for several radiohalides were established. Selected drugs were evaluated in vitro, and in vivo in normal mice (wild type control) and B6C3-g(APPswe,PSEN1dE9) 5Dbo/J transgenic mice (AD mice). **Results:** Syntheses, at the macro- and no-carrier added scale, physicochemical characterization and structure-activity studies for twelve *cyclo*Saligenyl-phosphotriesters have been completed. By varying substituents on the phenyl and carbohydrate residues, four compounds were designed that bind selectively and exclusively to BChE, either as a mixture of diastereoisomers or as their corresponding, resolved diastereoisomers. Further structural refinements provided a pair of diastereomers of which one exhibits strong and exclusive binding to BChE (IC50 = 50.1 " 1. 4 nM), whereas the second does not bind to BChE at all (IC50 >30,000 nM). All non-radioactive analogues and precursors needed for radiosyntheses of *cyclo*Saligenyl-phosphotriesters were synthesized and fully characterized. Radioactive compounds were also characterized and their strong, competitive and selective binding to BChE confirmed using electrophoresis methods. The separation of all radioactive compounds into their respective S_P and R_P diastereoisomers was also accomplished. Biodistribution and pilot nuclear imaging studies in normal (wild type) and AD mice were conducted to assist in the selection of the best candidate compounds for further studies. **Conclusions:** New reagents will be useful for longitudinal noninvasive assessment of BChE levels in Alzheimer's brain.

12

Correlation of the Ability to Perform the Activities of Daily Living (ADL) to a Density Index of Acetylcholine (ACh) Vesicular Transporters in the Striata of Women with Rett syndrome (RTT). J.R. Brašić, G. Bibat, K. Hiroto, A. Kumar, Y. Zhou, J.D. Hilton, M.B. Yablonski, A.S. Dogan; Johns Hopkins University, Baltimore, MD

Objectives: Rett syndrome (RTT) is a developmental disability characterized by mutations in the X-linked methyl-CpG-binding protein 2 (MeCP2) modified by X chromosome inactivation resulting in a wide range of phenotypes. (-)-5-[I-123]iodobenzovesamicol ([I-123]IBVM) provides the means to estimate a density index of acetylcholine (ACh) vesicular transporters in the living human brain by single photon emission computed tomography (SPECT). We hypothesize that the ability to perform the activities of daily living (ADL) is proportional to a density index of acetylcholine (ACh) vesicular transporters in the striata of women with RTT. **Methods:** Four women with RTT and nine healthy adult volunteer control participants underwent SPECT brain scans for sixty (60) minutes twenty-four (24) hours following the intravenous injection of 9 mCi [I-123]IBVM. The Vesicular Acetylcholine Transporter Binding Site Index (VATBSI), an estimate of the density of vesicular ACh transporters (Kuhl et al., 1994), was estimated in the striatum and the reference structures, the cerebellum and the occipital cortex.The women with RTT were assessed for ADL abilities by child neurologists with special competence in developmental disabilities. ADL abilities were rated utilizing a quantitative scale as follows: Activities of daily living score0 = cannot walk and cannot feed1 = walks with assistance and feeds self2 = walks without assistance and feeds self **Results:** Striatal VATSBI scored 5.2 + 0.9 in RTT and 5.7 + 1. 6 in healthy adults. There is no significant difference between the groups. In RTT striatal VATSBI and ADL scores are linearly associated (ADL = 0.89*VATSBI + 4. 5; R2=0.93; p<0.01; Figure 1). **Conclusions:** The ability to perform the activities of daily living (ADL) is correlated to a density index of acetylcholine (ACh) vesicular transporters in the striata of women with RTT. [I-123]IBVM may be a promising tool to characterize the pathophysiological mechanisms of RTT.

13

PET Measurement of 5-HT1A binding with [F-18]MEFWAY in the Nonhuman Primate. B.T. Christian[1], A.T. Hillmer[1], J.M. Moirano[1], N. Kalin[1], J. Mukherjee[2], M. Schneider[1]; 1. University of Wisconsin-Madison, Madison, Wisconsin; 2. University of California-Irvine, Irvine, California

Objectives: The 5-HT_{1A} receptor system has been shown to play an important role in many aspects of cognitive and emotional processing. Disruptions in this system are implicated in a wide variety of neuropsychiatric illnesses. [F-18]Mefway is a novel PET radioligand with high affinity and selectivity for the 5-HT_{1A} receptor system. The objective of this work is to present preliminary in vivo assessment of [F-18]mefway. **Methods:** Dynamic PET studies were acquired in 3 anesthetized rhesus monkeys using a high resolution microPET P4 scanner. Bolus injection studies were performed comparing the in vivo kinetics of [F-18]mefway and [C-11]WAY100635. Time activity curves were extracted from the high binding regions of the cingulate gyrus (CG) and mesial temporal cortex (MTC) and from the cerebellum, a region with very low specific binding, to obtain estimates of binding potential (BP_{ND}) using MRTM. Multiple injections (MI) studies with competing blocking doses of mefway have also been performed to assess displacement of [F-18]mefway. **Results:** Both [F-18]mefway and [C-11]WAY displayed high uptake in the regions of the MTC, raphe nuclei and CG and rapid clearance in the cerebellum. Intermediate levels of binding were seen throughout many of the cortical regions with higher levels in the insula and entorhinal cortices. BP_{ND} values were 5.6 and 6.5 in the CG, 7.2 and 7.0 in the MTC for mefway and way, respectively. The kinetics of both radiotracers were very similar throughout the regions of brain. MI studies of [F-18]mefway demonstrated significant displacement of radiotracer with a blocking dose of 200 nmoles. There was also no presence of uptake of defluorinated compound in the bone. **Conclusions:** The binding profile of [F-18]mefway is in very close agreement with [C-11]WAY, providing adequate imaging signal throughout the course of the PET experiment. [F-18]Mefway PET imaging holds great promise for studying the 5-HT1A receptor system in the brain.

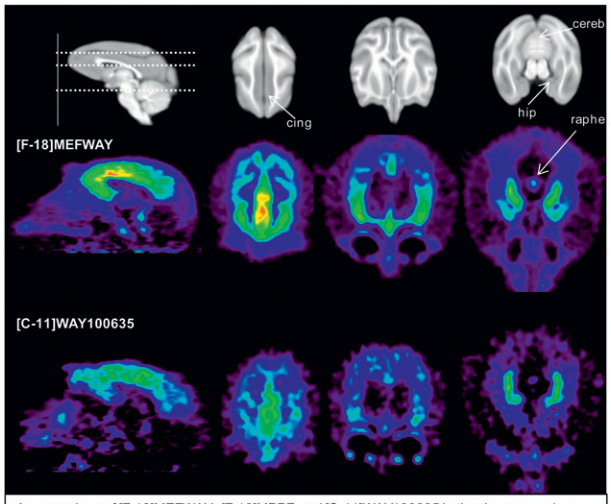

A comparison of [F-18]MEFWAY, [F-18]MPPF and [C-11]WAY100635 in the rhesus monkey brain. The top row is a skull stripped T1 MRI, with the dotted line illustrating the planes of the 3 transaxial slices highlighting radiotracer binding. All scans were acquired in the same rhesus monkey one week apart, with an injection of 1.4mCi . The images represent integrated activity from 8-120 minutes and are globally scaled to indicate comparative uptake (the PET images are not skull stripped).

14

Simultaneous SPECT / MRI Feasibility Demonstration. J. Hugg[1], D. Wagenaar[1], D. Meier[1], M.W. Benjamin[2], O. Nalcioglu[3], B. Patt[1]; 1. Gamma Medica-Ideas, Northridge, CA; 2. Johns Hopkins University, Baltimore, Maryland; 3. University of California, Irvine, California

Objectives: Demonstrate feasibility of simultaneous SPECT and MRI in a small animal prototype system as a proof of concept prerequisite for scale-up to human brain applications, including neuro-degenerative diseases and psychiatric disorders. **Methods:** We designed, built, and tested a complete SPECT/MRI prototype for insertion into a 12 cm MRI gradient coil cylindrical borehole. The T/R quadrature RF birdcage coil for MRI is integrated into the stationary SPECT detector, which uses solid-state pixilated CZT gamma detectors and a multiple pinhole collimator. The detectors are arranged in three rings of eight CZT modules each. One pinhole is associated with each 1. 6 mm pitch, 16 x 16 pixel detector module (eV Products). The cylindrical collimator was formed from tungsten powder and epoxy using a rapid prototyping method. Image reconstruction used sparse-view MLEM/OSEM with geometric detector-collimator response modeling. **Results:** The SPECT system has no apparent effect on MR imaging, including both gradient-echo and spin-echo sequences. Because the SPECT collimator is non-conducting, it does not support magnetic gradient-induced eddy currents. As expected, the magnetic field exerts a Lorentz force on the charge cloud created when a gamma photon interacts within a CZT detector. At 3 Tesla the mean displacement is about one pixel (1. 6 mm). The full detector-collimator response model accounts for this Hall Effect, which depends on magnetic field strength and depth of interaction. The first prototype has spatial resolution and geometric efficiency for 2. 0 mm diameter pinholes are 4. 7 mm and 1. 2 %, and for 1. 3 mm pinholes are 3. 3 mm and 0.5 %. The figure shows fused MR / Tc-99m SPECT images of mouse torso (MIBI) and dynamic renal uptake (DTPA) over 100 s (1. 6 s bins of list-mode data). **Conclusions:** Dynamic simultaneous SPECT/MR imaging is feasible with high detection efficiency using this stationary MR-compatible SPECT prototype system. Performance will be substantially improved in the next generation small-animal SPECT/MRI system by modifying the pinhole size and geometry, the detector, the collimator design, and the reconstruction algorithm. We plan to design and build a human brain simultaneous SPECT/MRI system, based upon the success and lessons learned from the prototype small-animal system.NIH grants R44EB6712 and R01EB8730 are gratefully acknowledged.

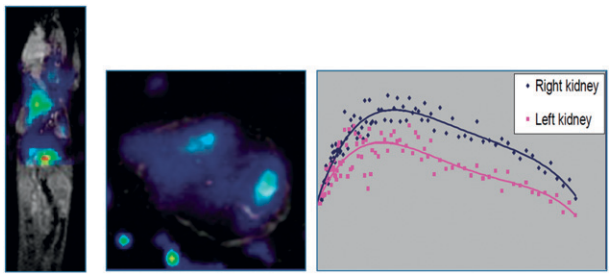

FIGURE 1. Brain simultaneous SPECT/MRI feasibility demonstration

15

Molecular and metabolic pattern classification for diagnosis of recurrent brain gliomas using support vector machine learning model.
F. Imani, F. Boada, F. Lieberman, C. Laymon, E. Deeb, J.M. Mountz; University of Pittsburgh Medical Center, Pittsburgh, PA

Objectives: The support vector machine (SVM) generates a separating hyperplane in an n-dimensional space between two classes of data (e.g., positive vs. negative). **Methods:** Twelve post-therapy patients (5 m, 7 f, 25–70 y), initially with histology proven gliomas (6 grade II and 6 grade III) who presented with contrast enhancing lesions on MRI and clinical symptoms suggestive but not conclusive of recurrence were selected. FDG uptake of lesions was rated 0 (no uptake), 1 (<WM), 2 (=WM), 3 (>WM, <GM), 4 (=GM), 5 (>GM). Choline (Cho) over Creatine (Cr) ratios of the lesions were normalized to the contralateral hemisphere. Clinical follow-up (>12 mo) and sequential MRI studies were used as the reference standard. An SVM with linear classifier without transformation into feature spaces (dot kernel) was established and computed using quadratic programming to maximize the distances between the hyperplane to the closest points of either class (supporting vectors). Given two parameters and dot kernel, a straight line could represent the hyperplane. Receiver operating characteristic (ROC) plots and optimal cutoff values for FDG uptake and Cho/Cr were calculated. **Results:** The SVM with 4 supporting vectors was able to classify all recurrent cases (n=8) without false findings (accuracy 100%). The equation of maximal margin separating hyperplane was 0.5F+0.86C=2. 23, where F and C represent FDG uptake and normalized Cho/Cr ratio, respectively. The accuracy of PET and MRS based on optimal cutoff values (FDG 2. 5 and Cho/Cr 1. 455) using ROC analyses were 83% and 75% respectively. **Conclusions:** SVM outperform single-parameter cutoffs in multimodal imaging for recurrent glioma detection using FDG PET and Magnetic Resonance Spectroscopy (MRS). SVM technique, in spite of small number of cases, was able to effectively combine MRS and FDG PET data and successfully classify recurrent gliomas more accurately than single-parameter cutoffs.

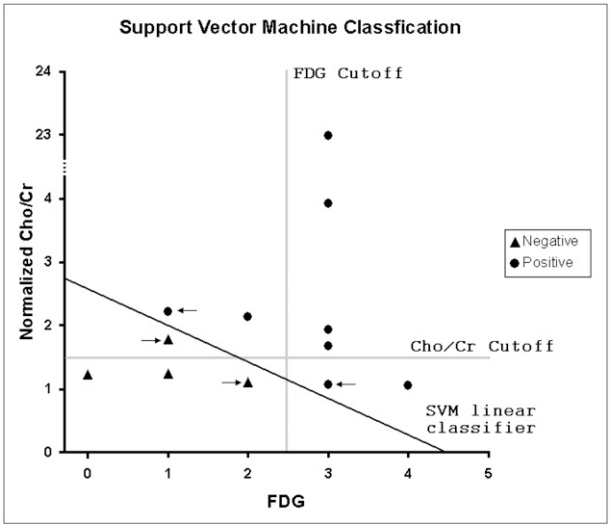

FIGURE 1. Recurrent glioma classification by calculated cutoff values from ROC analysis of FDG PET and normalized Cho/Cr MRS data, as well as SVM classification of the combined data. The arrows point to the supporting vectors.

16

a-[^{11}C]Methyl-L-tryptophan PET in Human Gliomas: Relationship to Tumor Proliferation, Glioma Type and IDO Expression.
C. Juhasz[1], P.K. Chakraborty[1], D.C. Chugani[1], O. Muzik[1], M. Sandeep[1], G.R. Barger[1], I. Zitron[2], C.E Batista[1], W.J. Kupsky[1]; 1. Wayne State University, Detroit, Michigan; 2. Karmanos Cancer Institute, Detroit, Michigan

Objectives: a-[^{11}C]Methyl-L-tryptophan (AMT) is a PET tracer for tryptophan metabolism to serotonin and via the immuno-modulatory kynurenine pathway. Accumulation of AMT and expression of indoleamine 2,3-dioxygenase (IDO), the rate-limiting enzyme of the kynurenine pathway, suggest a role of abnormal tryptophan metabolism in brain tumors. In this study, we analyzed kinetics of AMT in gliomas and correlated kinetic PET variables with tumor proliferative activity, glioma type and IDO expression. **Methods:** Thirty patients (mean age: 43 years) with a newly diagnosed glioma (WHO grade II-IV) underwent dynamic AMT PET scanning followed by surgical resection. AMT kinetic variables, including the unidirectional uptake rate (K-complex) and volume of distribution (VD; which characterizes tracer transport), were measured in the tumors, using a graphical approach from tumor dynamic PET and blood-input data, and AMT metabolic rates (k_3') were calculated. Tumor/contraletaral cortex ratios were also calculated for all kinetic variables. The PET kinetic values were correlated with tumor proliferative index (PI, measured from Ki-67 staining) and also compared between low-grade astrocytic tumors (pure astrocytomas and mixed gliomas) vs. oligodendrogliomas. IDO expression was assessed by immunohistochemistry in a subset of tumors. **Results:** Increased tumor/cortex ratios for K-complex [mean: 1. 59±0.74 SD] and/or VD [mean: 2. 01±1. 09 SD] were found in 29/30 tumors. Only one grade II oligodendroglioma showed no elevation in AMT kinetic parameters. Tumor PI showed a strong positive correlation with tumor VD values ($r=0.67$; $p<0.001$; Spearman's rank correlation) and tumor/cortex VD ratios ($r=0.78$, $p<0.001$) but not K-complex values or ratios ($p>0.8$). In the subgroup of low-grade (grade II) tumors, astrocytic tumors (n=8) could be differentiated from oligodendrogliomas (n=8) by higher k_3' tumor/cortex ratios (1. 65±0.46 vs. 0.96± 0.21; $p=0.002$). Widespread expression of IDO was seen in low-grade astrocytic tumors showing high k_3' ratios. **Conclusions:** AMT PET is very sensitive for the detection of both low- and high-grade gliomas. Increased AMT uptake can occur due to both increased transport and metabolism in gliomas. AMT transport kinetic values are highly predictive of tumor proliferative activity. High AMT metabolic rates in astrocytic tumors are likely related to increased metabolism of tryptophan via the kynurenine pathway, a potential target for tumor immuno-therapy.

17

Cannabinoid CB1 Receptors Imaging In Vivo in Schizophrenia by Positron Emission Tomography.
D.F. Wong, H. Kuwabara, A. Horti, J. Brasic, N. Cascella; Johns Hopkins University, School of Medicine, Baltimore, Maryland

Objectives: To determine the efficacy and utility of C-11 OMAR (also known as JHU 75528) for *in vivo* PET imaging of the cannabinoid CB1 receptor. We also test the utility of C-11 OMAR in investigating normal aging as well as to examine the cannabinoid system in normal controls as

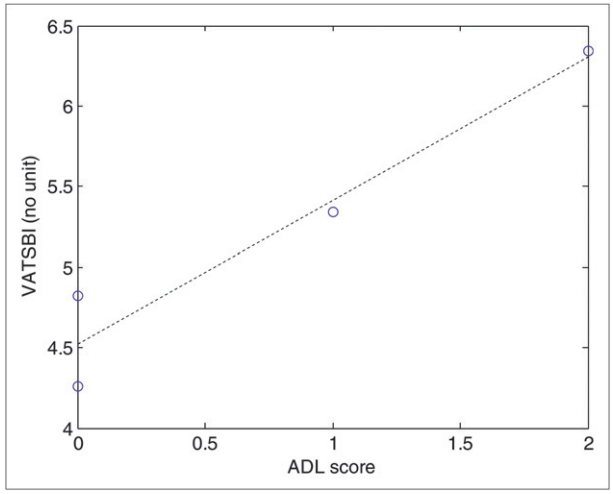

FIGURE 1. Vesicular Acetylcholine Transporter Binding Site Index (VATBSI) as a function of activities of daily living (ADL) score for four women with Rett syndrome (RTT).

well as patients with schizophrenia. **Methods:** The HRRT (high resolution research tomograph) (spatial resolution 2mm) was used in PET imaging studies in 10 controls and 7 patients with a DSM-IV diagnosis of schizophrenia, and no history of cannabis abuse or drug dependence. After an IV bolus of of 703 mBq of high specific activity C-11 OMAR, HRRT PET scans were carried out. All subjects also received an SPGR MRI (GE Sigma 1. 5T) MRI for anatomical coregistration, radial arterial blood sampling and HPLC metabolite analysis of the radiotracer. The method of Logan, 1996 (PRGA) as well as 2 tissue compartment model with constraint using 5 parameters (TTCM-5C) were used to calculate V_T in various brain regions. **Results:** In healthy controls, V_T ranged from1-1. 7 in various cortical/subcortical regions, with the highest binding in globus pallidus, cingulate and putamen. Among the controls, C-11 OMAR binding had a significant negative correlation with age and this effect was most significant in the globus pallidus. Among patients with schizophrenia, there was elevated binding across all regions when compared to the controls, most significantly in the globus pallidus ($p = 0.003$) when compared to 95% prediction limits of the linear regression of V_T vs. age. We found a significant correlation between V_T and the ratio of the BPRS psychosis to withdrawal score in frontal lobe (r^2=0.61), cingulate gyrus (r^2=0.60), parietal cortex (r^2=0.64) and putamen (r=0.58). **Conclusions:** These studies show the ability to image CB1 receptors in vivo, including patients with schizophrenia. These initial findings show promise of a relationship between some clinical characteristics and CB1 levels. This together with previous studies post mortem may help further understand the role of the CB1 cannabinoid receptor in schizophrenia.

18

Amygdala lesions eliminate emotional modulatory feedback to the visual cortex: a functional MRI study. B. Xu[1], F. Hadj-Bouziane[1], N. Liu[1], C. Wilson[2] , R. Tootell[1], L. Ungerleider[1]; 1. National Institute of Health, Bethesda, MD; 2. Boston University, Boston, MA

Objectives: Dextran-coated iron oxide nanoparticles, as functional MRI agents, have emerged as a routine tool for human neuroscience research and have been tested in several human clinical trials. The Imaging Probe Development Center as part of the NIH Roadmap Initiative dedicated to the production of molecular imaging probes, has produced a variety of nanoparticles in the past few years including liposomes, dendrimers, gold nanoparticles and reduced dextran-coated iron oxide nanoparticles. Dextran-coated iron oxide nanoparticles produced at IPDC and used in this work have a core size of 4. 37 ± 0.59 nm and a Z-average hydrodynamic diameter of 30 nm for functional MRI study. **Methods:** We initiated selective amygdala lesions in monkeys using a stereotaxic approach combined with injection of ibotenic acid. We used fMRI to compare the valence effects within the visual cortex in these amygdalectomized animals to the effects in control animals. Four different facial expressions were tested in a blocked design: neutral, aggressive, fearful and appeasing. Face-selective regions were identified in the inferior temporal (IT) cortex in both the controls and the amygdalectomized monkeys. **Results:** In controls, faces with emotional expressions produced enhanced responses in these regions relative to neutral faces, as expected. Fear grimace expressions consistently elicited the greatest responses. In monkeys with amygdala lesions, the valence effects within the visual cortex were greatly disrupted. The most striking demonstration of this disruption was found in the hemisphere with the most complete amygdala lesion. In this hemisphere, although face-selective patches were found in IT cortex, their activity was not modulated by facial expressions. Conversely, in three hemispheres with spared tissue in the anterior part of the amygdala (which was activated by neutral faces and modulated by facial expressions), the valence effects in the face-selective patches of IT cortex were present. Just as in controls, in these hemispheres with anterior amygdala sparing, fear grimace expressions evoked the greatest response. **Conclusions:** Overall, our data demonstrate that the amygdala is the source of the valence modulatory effects seen in the visual cortex.

19

Multi-Modal Molecular Imaging for Mild Traumatic Brain Injury. P.H. Yeh[1], T. Oakes[1], J. Graner[1], B. Wang[1], H. Pai[1], F. Munter[2]; 1. Henry Jackson Foundation for Military Medicine, Rockville, MD; 2. Walter Reed Army Medical Center, National Capital Neuroimaging Consortium, Departments of Radiology and Radiological Sciences, Uniformed Services University, Washington, District of Columbia

Objectives: Brain regions showing a strong temporal coherence during resting state are referred to as the "default mode network" (DMN), which reflects intrinsic properties of functional brain organization. Diffuse axonal injury (DAI) refers to white matter (WM) damage arising from the force of head injury. We hypothesize that the disrupted WM tracts impair DMN connectivity in TBI patients. The goal of this study is to assess the DMN using multimodal imaging techniques by identifying simultaneously independent components of each modality and the relationships between them. **Methods:** Participants included 7 documented male mild TBI patients (age 25.8±5.9 years, 68.1±26.0 days out from injury). PET-FDG scans, 3T DTI and dynamic susceptibility contrast MRI were acquired. DTI-derived measures (FA, MD) and MRI-contrast measures for CBF and CBV were estimated. All images were transformed to a MNI template using subject-specific T1W and T2W data. We applied parallel independent component analysis (ICA) by maximizing independence between two different modalities Participants included 7 documented male mild TBI patients (age 25.8±5.9 years, 68.1±26.0 days out from injury). PET-FDG scans, 3T DTI and dynamic susceptibility contrast MRI were acquired. DTI-derived measures (FA, MD) and MRI-contrast measures for CBF and CBV were estimated. All images were transformed to a MNI template using subject-specific T1W and T2W data. We applied parallel independent component analysis (ICA) by maximizing independence between two different modalities and their relationship concurrently. The ICA algorithm loading parameters were computed, and a correlation value was calculated between two modalities' component across subjects. A term linking the two modalities that optimally assesses the relationship between the two was estimated. Finally each unmixing matrix for both modalities was computed using information derived from both modalities (thresholded at a $|Z| > 2.5$). **Results:** Fig. 1 shows the mean images of 7 participants. Parallel ICA identified 7 significant paired independent components. Fig. 2 shows the three possible independent DMN networks of TBI, and the z-scores of the component maps, which mainly consist of dorsolateral, medial prefrontal, anterior and posterior cingulate, lateral parietal, MTL, cerebellum, and thalamus of the typical DMN regions. High FDG uptake was correlated with high CBF, high CBV, high FA and low MD in occipital and parietal lobes, but low FA and high MD in cerebellum (Fig. 2A). Low FA and high MD mainly in medial prefrontal region was associated with CBF and CBV changes in subcortical and occipital regions, and high FDG uptake in prefrontal and temporal regions (Fig. 2B). Low FA and high MD in corpus callosum was correlated with low FDG uptake, low CBF and CBV, especially in the regions of medial prefrontal, anterior cingulate, medial/inferior temporal and MTL of DMN network (Fig. 2C). **Conclusions:** These preliminary results suggest disrupted WM integrity, which is likely due to DAI, in the cortical-subcortical, cortico-cortical, and inter-hemispheric circuitry may impair DMN of TBI patients. Further investigations are needed with a much larger sample size and importantly, with a group of non-TBI control subjects.

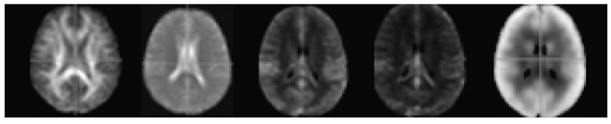

FIGURE 1. (From left) Mean FA, MD, CBF, CBV, and FDG images

20

Functional MRI characterizing phenotypic variation associated with Pten loss in a transgenic mouse glioma model. D. Zhao, C.H. Kwon, T. Soesbe, H. Zhou, R. Mason, L. Parada; University of Texas Southwestern Medical Center, Dallas, Texas

Objectives: We previously reported a transgenic mouse glioma model by inactivating tumor suppressor genes, Nf1 and p53 (Mut3). With further introduction of haploinsufficiency of Pten gene, which is frequently found in malignant glioma patients, we have recently shown that the more aggressive glioma phenotype developed (Mut4). Utilizing this glioma model that exhibits discernible features of the human counterpart, in the present study we evaluated the usefulness of functional MRI to characterize phenotypic variation of the gliomas due to loss of a Pten gene. **Methods:** Mut3 glioma (n = 4; *GFAP-cre*; $Nf1^{f/+}$; $p53^{-/+}$) and Mut4 glioma (n = 6;

GFAP-cre; *Nf1*$^{f/+}$; *p53*$^{-/+}$, *Pten*$^{loxp/+}$) were used in this study. Diffusion-weighted (DW) MRI was performed to assess tumor cellularity based on measurement of apparent diffusion coefficient (ADC) of free water molecule. Blood oxygen level dependent (BOLD) MRI was applied to evaluate response of the gliomas to carbogen breathing. **Results:** Our data showed that mean ADC of the Pten-deficient Mut4 gliomas (9.9 ´ 10^{-4} mm^2/s) was significantly lower than that of the PTEN-intact Mut3 gliomas (12. 9 ´ 10^{-4} mm^2/s; $p < 0.02$). Moreover, there was an inverse correlation between the mean ADC and Ki67 index, the proliferation marker, in the pooled Mut3 and Mut4 gliomas ($r > 0.8$; $p < 0.02$). The average decrease in transverse relaxation rate (R_2^*) in tumor regions was not significant for both the groups (mean Mut3 = - 0.3 ± 2. 7 s^{-1}, Mut4 = - 1. 2 ± 0.7 s^{-1}; $p > 0.3$). However, largely heterogeneous responses were observed intratumorally and intertumorally. Intriguingly, in contrast to decreased R_2^* observed in intratumoral regions and normal brains, significant increase in R_2^* with carbogen was found in peritumoral regions ($p < 0.05$). **Conclusions:** Our results suggested that non-invasive DW MRI and BOLD MRI may provide useful information for characterization of glioma molecular subtypes.

21

Synthesis of ^{68}Gallium-DOTANOC and Its Role in Malignancies of Brain. S. Lata, S. Singla, A. Kumar, A. Malhotra, S. Medhavi; Department of Nuclear Medicine and PETAll India Institute of Medical Sciences, New Delhi, Delhi, India

Objectives: 1. Synthesis of ^{68}Gallium(^{68}Ga)-DOTANOC and its Quality Control. 2. PET imaging of Brain tumors using ^{68}Ga-DOTANOC. **Methods:** ^{68}Germanium/^{68}Gallium generator was eluted with 5-8ml of 0.1MHCl to obtain radio-gallium (^{68}Ga). The eluant was concentrated by loading onto a cation exchanger cartridge. Furthermore impurities were removed by passing 1ml of 80% acetone/0.15M HCl solution. Thereafter, the pre-concentrated and purified ^{68}Ga was eluted with 400µl of 97.7% acetone/0.05M HCl. This was directly transferred to the reaction vial containing 30-50µg of DOTANOC. Synthesis was carried out for 10 minutes at 90-95°C followed by purification of labeled peptide on reverse phase C-18 column. The purified ^{68}Ga-DOTANOC was extracted from the column using 1ml of 50% ethanol and transferred to the production vial. The obtained product was then diluted with 10ml normal saline. This procedure was completed in 25-30 minutes. Quality control parameters (color, pH, Rf, Radiochemical purity and % yield) were recorded before injecting ^{68}Ga-DOTANOC in patients. Approximately 4mCi (148MBq) of above preparation was injected intravenously in patients and imaging was done one hour post injection on a dedicated PET/CT scanner ^{68}Ga-DOTANOC preparation was a clear and colorless solution with pH-6.5-7.0, Rf-0.0. Radiochemical Purity >99% and 70-85% yield. **Results:** An excellent target to non-target ratio was achieved in images of patients. **Conculsions:** ^{68}Ga-DOTANOC can be synthesized easily with excellent reproducibility and good yield. This can be used in imaging of Meningioma, Medulloblastoma, Astrocytoma and a rare entity called Primary Brain Carcinoid. Further advantage of diagnosing the presence of SSTR would be targeting these tumors with PRRT and assessment of response on serial imaging.

22

A comparative study of anatomical 3T and 7T MRI imaging of malignant brain tumors using ultrasmall superparamagnetic iron oxide (USPIO) nanoparticles and gadolinium-based contrast agents. S.B. Tuladhar, E. Dosa, C. Lacy, M. Haluska, S. Gahramanov, J. Njus; Oregon Health & Science University, Portland, Oregon

Objectives: The purpose of this study is to compare the contrast agent detection sensitivity between 3T and 7T MRI instruments. Ten patients with histologically-confirmed primary malignant tumors participated in the study. MRI were acquired at 3T (Siemens TIM) and 7T (Siemens MAGNETOM). **Methods:** Each subject was scanned on 3 consecutive days. Subjects received a total dose of 0.1 mmol/kg of a gadolinium based contrast agent (Gd) on day 1 and 4 mg/kg of an USPIO-Ferumoxytol (Fe) on day 2. Two measures were calculated from 3T and 7T anatomical scans for each subject: 1) absolute signal enhancement difference between pre- and post-contrast tumor enhancing areas normalized to precontrast signal enhancement; the contrast enhancement ratio (CER) and 2) enhancement volume for T_2W MPRAGE. We calculated the CER for 3T and 7T images acquired using both contrast agents. **Results:** The mean CER using Gd on 3T MPRAGE images was 1. 53 ±0.96 (SD); on the 7T MPRAGE, it was 3. 28 ± 2. 07 (SD) – a significant difference ($p<0.002$). The mean CER of Fe-enhanced images was 1. 27±0.68 (SD) and 1. 23±0.81 (SD) on 3T MPRAGE and 7T MPRAGE, respectively. T_1W enhancement volume in 7T post-Gd MPRAGE images was not significantly different than in 3T images (7T: 10.80cm^3 ± 11. 90(SD), 3T: 9.95cm^3 ± 10.63(SD) $p = 0.36$). For post-Fe MPRAGE images, T_1W enhancement volume in 3T was significantly higher than in 7T images (7T: 1. 16cm^3 ± 1. 18(SD), 3T: 2. 73cm^3 ±2. 51 (SD), $p = 0.01$). The mean values of CER and enhancement volume for Gd-enhanced T_1W MPRAGE were higher at 7T compared to 3T, likely the result of increased nominal water proton T_1 values at 7T. This initial finding suggests that for this acquisition Gd detection sensitivity is higher at 7T than 3T.**Conclusions:** As Gd-based contrast agents are the standard for identifying tumor areas with high vascular permeability, 7T MRI appears to offer advantages in this regard. Alternatively, it may be possible to obtain the same clinical information at 7T with lower Gd dose than at 3T. Fe detection sensitivity in T_1W MPRAGE images was superior at 3T, likely due to increased 7T T_2* signal quenching from tumor accumulated Fe which attenuated T_1W enhancement. Our ongoing study shows that ferumoxytol-enhanced 7T T2*W images seems to be better for blood vessel visualization in comparison to the Fe-3T T2*W images.

23

Production and Preliminary Testing of Ultra-Stable Gadolinium-Benzyl-DOTA-Cholera Toxin B Conjugates as MRI Brain Circuitry Tracking Agents. O. Vasalatiy, C.W.H. Wu, S. Cheal, R.B. Tootell, A.P. Koretsky, G.L. Griffiths , L. Ungerleider; National Institutes of Health, Rockville, Maryland

Objectives: Cholera toxin subunit B (CTB) is a useful agent for MRI imaging of brain circuitry by virtue of its transport properties. CTB labeled with gadolinium (Gd) might allow us to non-invasively image neuronal connections over extended time periods. Moreover it may have advantages over low molecular weight Gd complexes of DOTA-biotin, or manganese chloride. Gd in an ultra-stable chelated form, bound to CTB by a bifunctional version of the macrocyclic chelating agent 1,4,7,10-tetraazacyclododecane-N,N',N'',N'''-tetraacetic acid (DOTA), should represent an optimum CTB contrast reagent useful for multi-day tracking, by virtue of this stability. **Methods:** The Gd complex of the 4-isothiocyanatobenzyl-DOTA preactivated bifunctional chelate was prepared and covalently coupled to CTB at Gd-chelate: CTB ratios of 1. 4 to 4. 0, as we sought to balance maximum Gd content for ideal signal detection with maximum retention of CTB biological transport activity. **Results:** Conjugates were comprehensively characterized for protein concentration and Gd content by MADLI-TOF, HPLC and ICP-MS, and the reagent's physical and *in vitro* properties will be described. Agents were injected into a Sprague-Dawley rat model for tracing studies and showed target-specific neuronal transport of Gd-DOTA-CTB. **Conclusions:** Gd-DOTA-CTB represents a promising new agent for further brain circuitry tracking studies.

24

Radiosynthesis of [^{18}F]FE@PBM, a novel potential PET radioligand for the norepinephrine transporter. W. Wadsak[1], J. Ungersboeck, A. Hoepping[2], M. Mitterhauser[1], R. Lanzenberger[1], K. Kletter[1]; 1. Medical University of Vienna, Department of Nuclear Medicine, Vienna, Austria; 2. Advanced Biochemical Compounds, Radeberg, Germany

Objectives: Reboxetine (2-[a-(2-ethoxyphenoxy)-benzyl]-morpholine) is known to be a selective antagonist at the norepinephrine transporter (NET) since 1984. Because of its excellent affinity and selectivity for the norepinephrine transporter it was chosen as lead compound for the design of NET-specific radiopharmaceuticals both for PET- and SPECT-imaging. So far, the application of the reboxetine derivatives, (*S*,*S*)[^{11}C]MeNER ([^{11}C](*S*,*S*)-2-(a-(2-methoxyphenoxy)-benzyl)morpholine) and [^{18}F]FMe-NER-d_2 was described. Recently, PBM ((2*S*,3*S*)-2-[a-(2-(carbomethoxy) phenoxy) benzyl]morpholine) was introduced as another promising

NET-PET-candidate with similar or superior affinity for hNET (K_i=1. 32nM) and selectivity over hSERT and hDAT (K_i=614nM and K_i>3000nM, respectively) compared to (*S*,*S*)-reboxetine or (*S*,*S*)MeNER. (Zeng et al. Bioorg Med Chem 2008;16:783). Evaluating the structure-activity relationships, we concluded that a reboxetine derivative bearing a fluoroethyl-ester moiety ([^{18}F]FE@PBM) should be the ideal compound, combining high affinity and NET-selectivity as well as metabolic stability. Hence, the aim of this work was the radiosynthesis of the novel potential NET-PET-ligand, [^{18}F]FE@PBM. **Methods:** [^{18}F]FE@PBM was synthesized using an optimized two-step fluoroethylation method (Wadsak et al. Nucl Med Biol 2007;34:1019). [^{18}F]fluoride was azeotropically dried, 2-bromoethyl triflate was added and heated for 10min at 90°C. The intermediate, 1-bromo-2-[^{18}F]fluoro-ethane (BFE) was distilled and added to the TBA salt of the protected precursor (N-BOC-PBM-acid). Conversion was achieved at elevated temperature (100-150°C) within 30min and deprotection was performed with TFA. Radiochemical yields (RCY) were determined using radio-HPLC and radio-TLC. **Results:** So far, a dependence upon the precursor concentration was observed. At 4mg/mL, 65% RCY was observed. Using radio-TLC, the product (R_f 0.5-0.6) was separated from unreacted [^{18}F]fluoride (R_f 0-0.1) and an unknown by-product (R_f 0.7-0.8). The HPLC chromatogram showed only minor amounts of by-product formation (< 5%). **Conclusions:** We were able to prepare [^{18}F]FE@PBM with satisfactory yields within 55min. Further optimization and chromatographic purification are currently conducted and preclinical testing will start immediately afterwards. We are optimistic that [^{18}F]FE@PBM will soon prove to be a valuable NET-PET-tracer for broad use. The first step has definitely been taken successfully.

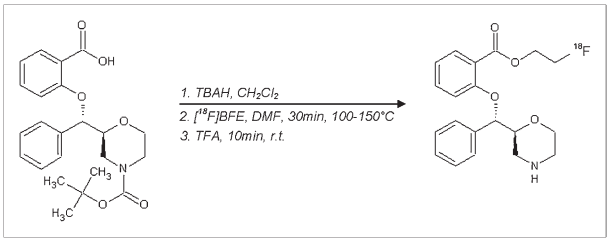

25

Human mesenchymal stem cells in treatment of intracerebral hemorrhage: an effectiveness study with primate models. Z. Zhu, M. Feng, W. Renzhi, F. Li; Department of Nuclear Medicine, Peking Union Medical College Hospital, Beijing, China

Objectives: This preclinical study was designed to evaluate human mesenchymal stem cells (hMSCs) obtained from bone marrow in treatment of intracerebral hemorrhage (ICH) in primate models. **Methods:** Twenty-four *Macaca fascicularis* monkeys (M, 4-6 y, 4. 2±0.2 kg) were enrolled. ICH models were built by stereo-guided injection of 1. 5 ml autologous arterial blood between the right cortex and basal ganglia. By stereo-guided method, (1-5) $\times 10^6$ hMSCs were transplanted surrounding the hematoma one week later (early treatment group, n=8) or 4 weeks later (late treatment group, n=8); saline was used instead to the control monkeys, either one week later (n=4) or 4 weeks later (n=4). All monkeys were evaluated weekly by neurological deficit scoring, 19 monkeys underwent serial FDG PET evaluation, and finally, all monkey brains were collected for pathological analysis. **Results:** Neurological deficit scoring showed the best recovery in early treatment group, followed by late treatment group and the controls. In serial FDG PET evalutaion, both early and late MSC-treated groups showed significant higher ^{18}F-FDG uptake at the basal ganglia region compared with the control group one week after hMSCs injection (*P* values were 0.019 and 0.022, respectively), representing early response to treatment. Eight weeks after hMSCs treatment when recovery reached a plateau, the recovery percentages of adjacent cortex and basal ganglia in early treatment group were significantly higher than those in the controls (99.5%±2. 4% vs 88.0%±2. 8% for adjacent cortex, P=0.004; 99.0%±4. 3% vs 91. 0%±1. 4% for basal ganglia, P=0.046); better recovery was also found in the late treatment group, but without significance. Pathological analysis revealed higher vessel density at the hematoma remains in both early and late hMSCs-treated monkeys (*P* values were 0.007 and 0.014, respectively). **Conclusions:** This preliminary study indicates that intracerebral transplantation of hMSCs may benifit the recovery of experimentally induced ICH in monkeys, and earlier treatment can lead to better result.

26

Parameter Optimization for Quantitation of Human Beta-Amyloid PET Scans. G. Zubal, G. Wisniewski, O. Barret, J. Batis, K. Marek, J.P. Seibyl; Institute for NeuroDegenerative Disorders, New Haven, CT

Using our in-house developed PC executable code, which automatically places regions of interest (ROIs) onto nuclear medicine brain scans for extracting PET quantitative beta-amyloid SUVr values, we evaluated the optimal use of normalizing templates and methods for masking white matter and CSF in order to obtain the best discrimination between normal and Alzheimer patient scans. Over 50 PET scans were downloaded from the ADNI website, representing a combined group of healthy controls and subjects with Alzheimer's Disease. Our Alzheimer's Disease Evaluation of Radiotracers software package (ADER): 1) reads the reconstructed images, 2) geometrically normalizes, in 3D, the subject's brain volume to a beta-amyloid PET template, 3) overlays the regions defined in the Automated Anatomical Labeled (AAL) template, 4) identifies areas of white and gray matter, and 5) uses predetermined ROIs from the AAL template to extract radiotracer brain uptake intensities to calculate regional SUVr values. When normalizing to the PET template, one of three templates may be selected; the variability between normalization results for these three templates is investigated. Elimination of white matter and CSF areas from the applied ROIs is accomplished by overlaying predetermined normalized pixel masks. An array of pixel masks is available, and their affect on final SUVr quantitation is determined. When compared to the analysis using interactively placed ROIs, ADER delivers human beta-amyloid concentrations with similar inter-rater variability as when the same PET scans are manually analyzed by human operators. The bias and variance of the ADER delivered automated analysis, compared to human manual analysis, is influenced by the selection of the normalization template and white/CSF pixel masks applied to the ROIs. This work is an extension of earlier work developed for analyzing iodinated beta-amyloid SPECT tracers [J Nucl Med. 2008; 49 (Suppl. 1): 378P]. ADER, our fully automated and non-subjective brain analysis software package: a) decreases processing time to evaluate beta-amyloid concentrations in human brains, b) points the way to an objective method for comparing clinical results across imaging centers, c) offers an evaluation method for testing other radiotracers targeting beta-amyloid. This automated objective software method has been tested and statistically compared to over 150 manual analyses of both PET and SPECT brain scans.